ELSEVIER

Finite Elements in Analysis and Design 26 (1997) 315–335

FINITE ELEMENTS IN ANALYSIS AND DESIGN

Superelements for the finite element solution of two-dimensional elliptic problems with boundary singularities

Zohar Yosibash[a,*], Bernard Schiff[b]

[a] *Pearlstone Center for Aeronautical Engineering Studies, Department of Mechanical Engineering, Ben-Gurion University of the Negev, P.O. Box 653, 84105 Beer-Sheva, Israel*

[b] *School of Mathematical Sciences, Raymond and Beverly Sackler Faculty of Exact Sciences, Tel Aviv University, Ramat Aviv, Tel Aviv 69978, Israel*

Abstract

A novel singular superelement (SSE) formulation has been developed to overcome the loss of accuracy encountered when applying the standard finite element schemes to two-dimensional elliptic problems possessing a singularity on the boundary arising from an abrupt change of boundary conditions or a reentrant corner. The SSE consists of an inner region over which the known analytic form of the solution in the vicinity of the singular point is utilized, and a transition region in which blending functions are used to provide a smooth transition to the usual linear or quadratic isoparametric elements used over the remainder of the domain. Solution of the finite element equations yield directly the coefficients of the asymptotic series, known as the flux/stress intensity factors in linear heat transfer or elasticity theories, respectively. Numerical examples using the SSE for the Laplace equation and for computing the stress intensity factors in the linear theory of elasticity are given, demonstrating that accurate results can be attained for a moderate computational effort.

Keywords: Finite element methods; Singularities; Stress intensity factors; Laplace equation; Elasticity

1. Introduction

The finite element method based on the primal weak form [1, Chap. 4], referred to as the potential energy formulation, or the the displacement formulation in elasticity, has become a leading tool for the solution of boundary value problems involving elliptic equations of second order. In many problems of practical importance, the solution possesses singularities at so-called singular points on the boundary, due, for example, to a reentrant corner or an abrupt change in the boundary conditions. The analytic form of the solution in the vicinity of a singular point is usually known in the form of an asymptotic series with unknown coefficients [2, 3]. In the presence of such singularities, the standard finite element scheme, in both its h- and p-variants, becomes very inaccurate,

* Corresponding author.

0168-874X/97/$17.00
PII S0168-874X(96)00088-1

and reasonable engineering accuracy is often impossible, or at least very costly to obtain [4, 5, Chap. 8]. The standard finite element methods have been modified in various ways in order to overcome this difficulty (see [6, 7] for surveys of the main ideas). The schemes suggested, however, suffer from one or more of three principal disadvantages. Some employ a very fine mesh in the vicinity of the singularities, requiring a large number of degrees of freedom, some need a kind of "post processor" to determine the coefficients of the asymptotic series from the solution vector (such as the effective auxiliary mapping method [8]), and some employ singular elements, which are difficult or even impossible to incorporate into standard finite element programs.

In the following we show how, for any type of singular point in a two-dimensional domain, these difficulties may be overcome in the h-scheme, provided only that the form of the asymptotic series for the solution in the neighborhood of the singular point is known *explicitly*. We introduce a singular superelement (SSE) to replace the usual elements over a region surrounding the singular point. This SSE is considerably different from, and much more general than the constrained superelement presented in [9]. It is divided into two regions. Over the internal region the correct analytic form of the solution is used explicitly for the trial functions. Over the transition region, blending functions are employed to provide a smooth match between the trial functions in the internal region and those used over the remainder of the domain. It has been designed so as to conform with linear or quadratic elements, so that standard linear or quadratic isoparametric elements may be employed over the remainder of the domain. The SSE can be a convex polygon of any shape, and may be incorporated into the finite element mesh in the same way as any other element. For example, the SSE described in [10] was incorporated successfully as a superelement into the popular commercial finite element code MSC/NASTRAN,[1] see [11]. The SSE has been employed to determine stress intensity factors for two-dimensional crack and V-notch problems in the linear theory of elasticity [10], yielding results of high accuracy for a moderate computational effort. In the current paper, we describe the method in detail, and present results for three "benchmark" problems in order to demonstrate its accuracy, efficiency and generality of application.

The method is outlined in Section 2. Details are given of the formulations for the case of the Laplace equation (including the determination of the coefficients in the asymptotic series), and for the calculation of the displacements and stress intensity factors for cracks under the assumptions of linear elasticity. Numerical examples showing the accuracy and efficiency of the method are presented in Section 3. The solution and series coefficients have been computed for the Laplace equation over an L-shaped region and for the "Motz Problem" for this equation, and the "Mode 1" stress intensity factor has been computed for a rectangular cracked plate under tension. The results of our computation are compared with those obtained by other methods. Our conclusions, together with suggestions for future extensions of the SSE concept, are given in Section 4.

2. The computational scheme

Let Ω be a two-dimensional domain with a boundary $\partial\Omega$ consisting of analytic simple arc curves called edges. These edges intersect at points called vertices. We shall be interested in cases where a boundary point is singular, either because $\partial\Omega$ has a reentrant corner there, or because the boundary

[1] The MacNeal-Schwendler Corporation, Los Angeles, CA.

conditions change abruptly as we pass through the point. We wish to solve the Laplace equation or the Navier equations of linear elasticity over Ω. We will first introduce the appropriate variational form for the problem in the form of the minimization of the total energy. We then formulate the usual Galerkin finite element approximation to minimize the energy over a finite-dimensional subspace. Finally, we modify the scheme by introducing SSE covering the region surrounding the boundary singularity to counteract the loss of accuracy in the neighborhood of such a point.

2.1. The scalar problem

Consider the strong formulation of the Laplace problem:

$$-\nabla^2 u(x, y) = 0, \quad (x, y) \in \Omega, \tag{1}$$

subject to the boundary conditions

$$u = g_1, \quad (x, y) \in \Gamma^{\mathrm{D}}, \tag{2}$$

$$\frac{\partial u}{\partial n} = g_2, \quad (x, y) \in \Gamma^{\mathrm{N}}, \tag{3}$$

where Γ^{D} and Γ^{N} are parts of $\partial\Omega$ of positive measure such that $\Gamma^{\mathrm{D}} \cup \Gamma^{\mathrm{N}} = \partial\Omega$, and $g_1 = g_2 = 0$ in the vicinity of any singular point of interest.

The variational principle associated with (1)–(3) can be stated as follows:

Seek $u \in \tilde{H}_{\mathrm{B}}(\Omega)$, which minimizes

$$I(v) = \frac{1}{2}a(v, v) - (g, v) \overset{\text{def}}{=} \frac{1}{2}\int\int_{\Omega}[(\nabla v)\cdot(\nabla v)]\,\mathrm{d}\Omega - \int_{\Gamma^{\mathrm{N}}} g_2 v\,\mathrm{d}s, \tag{4}$$

where $\tilde{H}_{\mathrm{B}}(\Omega) = \{u = \tilde{u} + \psi \mid \tilde{u} \in H^1(\Omega)\}$, $H^1(\Omega)$ being the usual Sobolev space of functions which, together with their first-order derivatives, are square-integrable over Ω and ψ is a fixed function satisfying the non-homogeneous boundary conditions over Γ^{D}.

We will approximate u of (4) by $u^h(x, y)$ which minimizes $I(v)$ over $\tilde{E}(h)$, a finite-dimensional subspace of $\tilde{H}_{\mathrm{B}}(\Omega)$, and will take this subspace to be one of the usual h-version. Towards this end we select a family of finite-dimensional subspaces $\tilde{E}(h)$ of $\tilde{H}_{\mathrm{B}}(\Omega)$, such that $\tilde{E}(h)$ are the usual h-version finite element spaces of low-order polynomials over a mesh of elements characterized by the largest element size of length h. In this case we have

$$\lim_{h\to 0} u^h(x, y) = u(x, y).$$

(See [5, Chap. 2] for details.)

We are thus using the equivalent of the Galerkin method, in which the spaces of the trial and test functions coincide.

2.2. The elastostatic problem

The two-dimensional strong formulation for the elastostatic problem is given by the Navier equations (see [12, p. 73]). The corresponding variational principle, associated with the elastostatic problem, analogous to (4), is given as follows:

Seek $\boldsymbol{u} \in \tilde{H}_B(\Omega) \times \tilde{H}_B(\Omega)$ such that

$$I(\boldsymbol{v}) = \frac{1}{2}a(\boldsymbol{v},\boldsymbol{v}) - (\boldsymbol{t},\boldsymbol{v}) \stackrel{\text{def}}{=} \frac{1}{2}\int\int_{\Omega}([D]\boldsymbol{v})^{\mathrm{T}}[E][D]\boldsymbol{v}\,\mathrm{d}\Omega - \int_{\partial\Omega}\boldsymbol{v}^{\mathrm{T}}\boldsymbol{t}\,\mathrm{d}s \tag{5}$$

is minimized, where $[E]$ is the material matrix and $[D]$ is a differential operator defined as follows:

$$[D] \triangleq \begin{bmatrix} \dfrac{\partial}{\partial x} & 0 \\ 0 & \dfrac{\partial}{\partial y} \\ \dfrac{\partial}{\partial y} & \dfrac{\partial}{\partial x} \end{bmatrix},$$

$\boldsymbol{u}$ is the vector of displacements, and $\boldsymbol{t}$ is the vector of the tractions applied over the boundary $\partial\Omega$.

2.3. The singular superelement

Notation. Let P denote the singular point. We construct a superelement in the form of a polygonal domain Ω_{poly} about P in the following manner. Let S_R be a disc, center P, of radius R small enough to be contained wholly in Ω_{poly}. Ω_R is denoted by $S_R \cap \Omega$ and the circular part of the boundary of Ω_R by Γ_R. Let Ω_p denote the part of Ω_{poly} between Γ_R and Γ_p, the outer boundary of Ω_{poly}. We will refer to Ω_R as the inner region of the superelement, and to Ω_p as the transition region. The remaining domain is defined as $\Omega_O = \Omega - \Omega_{\text{poly}}$. See Fig. 1.

We will now describe the choice of the trial functions over these two regions and the computation of the corresponding stiffness matrices. Let $u(x,y)$ be the solution of the scalar boundary value problem over Ω. It is well known that in the neighborhood of the singular point P, $u(x,y)$ may be represented by an asymptotic series (see [2]):

$$u = \sum_{i=0}^{\infty} A_i f_i(r,\theta,\alpha_i), \tag{6}$$

where f_i are known functions, α_i are real constants, A_i are expansion coefficients, and (r,θ) are polar coordinates with origin at the singular point.

Explicit expressions for f_i are provided in the following sections. For the elastostatic case, an analogous expression for $\boldsymbol{u}$ exists, except that f_i is a vector function $\boldsymbol{f}_i$, and the α_i may also be complex. Usually, f_i has an r-dependence of r^{α_i} and thus if the real part of α_i is less than 1, the value of ∇f_i becomes unbounded as r approaches zero, and the point P is referred to as being a singular point. $\alpha_{\min}$, the minimum value of α_i, characterizes the strength of the singularity, so that the most singular term in the expansion for the first derivative of the solution will have an r-dependence of $r^{\alpha_{\min}-1}$ as r tends to zero. It is known [4] that the solution u belongs to the fractional Sobolev space (for details see [3], Chap. 1) $H^{1+\alpha_{\min}}(\Omega)$, and if the usual finite element scheme is used without modification, the rates of convergence for the h-version and for the p-version are $h^{\alpha_{\min}}$ and $(1/p)^{2\alpha_{\min}}$, respectively, where the errors are measured in the energy norm, $||v||_E \stackrel{\text{def}}{=} \sqrt{a(v,v)}$, see [4, 5] (if $\alpha_{\min}$ is a positive integer, then one might need to adjust these rates with logarithmic factors, e.g. $(1/p)^{2\alpha_{\min}} \log p$).

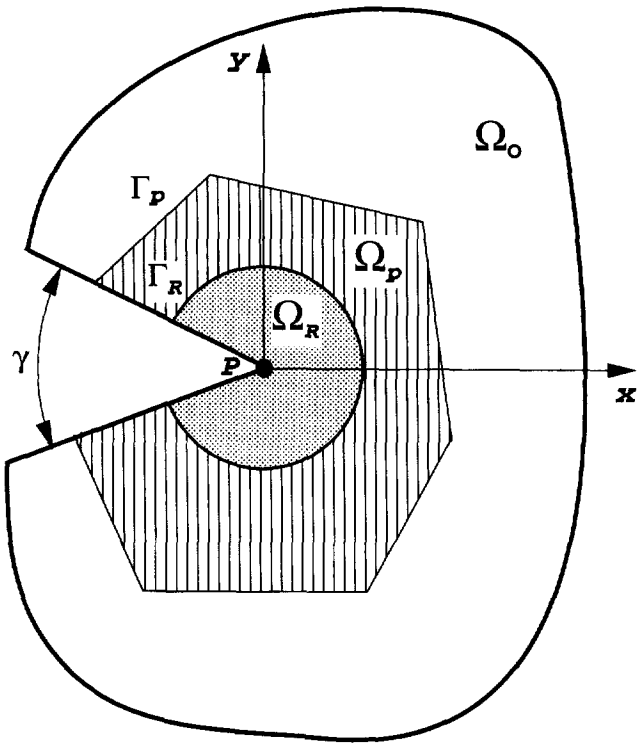

Fig. 1. Domain and notation.

We construct a conforming SSE over the domain Ω_{poly} by choosing the trial functions as follows. Over Ω_R, surrounding the singular point, the asymptotic expansion for the exact solution, suitably truncated, is used as the trial function. Over Ω_p, the transition region of the SSE, blending functions are employed to provide a smooth match between the asymptotic expansion used over Ω_R and the piecewise polynomials used as trial functions over Ω_O, the remainder of Ω.

As a consequence, the bilinear forms in (4) and (5) will be split into three bilinear forms, $a(v,v) = a_R(v,v) + a_p(v,v) + a_O(v,v)$, over Ω_R, Ω_p and Ω_O, respectively.

We now outline the computation for the region Ω_R. Over this region, the trial function space is taken to be a linear combination of the known functions $f_i(r,\theta,\alpha_i)$ presented in (6), so that the approximation over Ω_R is $u_{\text{FE}} = \sum_{i=0}^{N} A_i f_i(r,\theta,\alpha_i)$. The (i,j) term in the stiffness matrix corresponding to $a_R(u,u)$ is then given by

$$[a_R]_{ij} = \int_0^R \int_{-\pi+\gamma/2}^{\pi-\gamma/2} \left[\frac{\partial f_i}{\partial r}\frac{\partial f_j}{\partial r} + \frac{1}{r^2}\frac{\partial f_i}{\partial \theta}\frac{\partial f_j}{\partial \theta}\right] r \, dr \, d\theta, \quad i,j = 1,\ldots,N. \tag{7}$$

Note that the unknowns associated with $[a_R]$ are the first N coefficients of the asymptotic expansion in (6). The integrals in (7) were evaluated using 8×8 point tensor-product Gaussian quadrature. In view of the fact that in some cases the leading f_i (apart from the constant term) and its derivatives are singular at $r = 0$, some of the calculations were repeated using adaptive quadrature (NAG

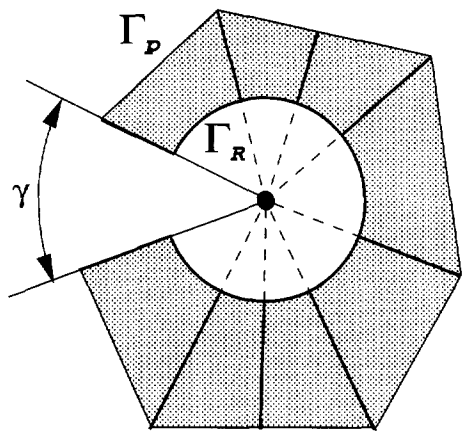

Fig. 2. Elements in Ω_p.

subroutine D01AJF) in the r-direction in order to check that the integrals had indeed been evaluated to sufficient accuracy.

We now deal with the transition region Ω_p. As we wish to develop a conforming finite element scheme, we have to ensure that Ω_p will be covered by some kind of elements in such a way that on Γ_R the trial functions go over continuously to function (6), whilst on the polygon Γ_p they should be polynomials compatible with the trial functions adopted over Ω_0. This is achieved by covering Ω_p with a single row of elements, each possessing three straight edges and one edge in the form of a circular arc lying on Γ_R (see Fig. 2). The elements in Ω_p are constructed as "transfinite elements" [13] and are mapped onto the standard element in the (ξ,η) plane by the bilinear blending transformation $\boldsymbol{T}(\xi,\eta) \stackrel{\text{def}}{=} (r(\xi,\eta),\theta(\xi,\eta))^{\mathrm{T}}$ of the form

$$\begin{aligned}\boldsymbol{T}(\xi,\eta) = {} & (1-\xi)\boldsymbol{T}(0,\eta) + \xi\boldsymbol{T}(1,\eta) + (1-\eta)\boldsymbol{T}(\xi,0) + \eta\boldsymbol{T}(\xi,1) \\ & -[(1-\xi)(1-\eta)\boldsymbol{T}(0,0) + (1-\xi)\eta\boldsymbol{T}(0,1) + \xi(1-\eta)\boldsymbol{T}(1,0) + \xi\eta\boldsymbol{T}(1,1)]. \end{aligned} \tag{8}$$

The expression $\boldsymbol{T}(\xi,0)$, for example, describes the mapping of side AB of the standard element onto the side ab in the (x,y) plane (see Fig. 3). Substituting for the mappings for each of the sides and vertices into (8), we obtain the following explicit expression for the bilinear blending transformation in polar coordinates:

$$\begin{aligned}\boldsymbol{T}(\xi,\eta) = {} & \begin{pmatrix} \{R_4^2 + \xi^2[R_5^2 + R_4^2 - 2R_4R_5\cos(\beta_2-\beta_1)] + 2\xi R_4[R_5\cos(\beta_2-\beta_1) - R_4]\}^{1/2} \\ \arctan\left(\dfrac{R_4\sin\beta_2 + (R_5\sin\beta_1 - R_4\sin\beta_2)\xi}{R_4\cos\beta_2 + (R_5\cos\beta_1 - R_4\cos\beta_2)\xi}\right) \end{pmatrix}\eta \\ & + \begin{pmatrix} R \\ \beta_2 + (\beta_1-\beta_2)\xi \end{pmatrix}(1-\eta). \end{aligned} \tag{9}$$

With this choice of $\boldsymbol{T}$, the Cartesian coordinates x and y will be linear functions of ξ along cd.

A typical element in Ω_p, and the transformation from the standard plane is shown in Fig. 3. The trial functions over Ω_p are linear or quadratic blending functions in such a way as to match

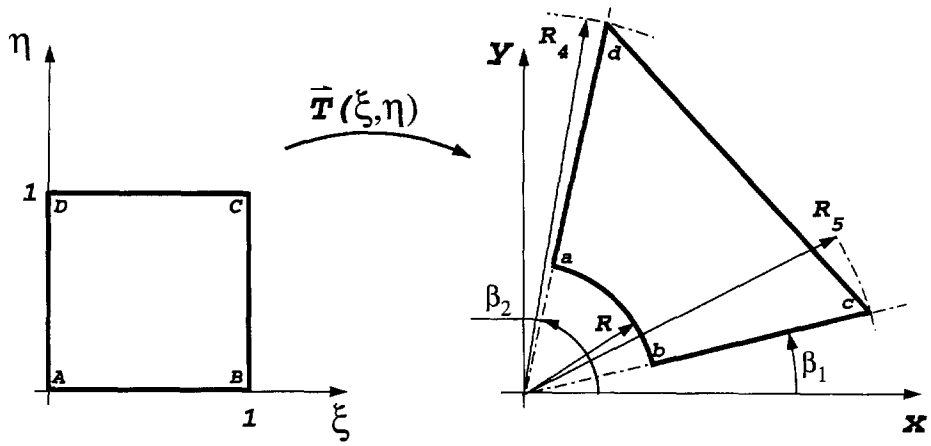

Fig. 3. A typical element in Ω_p, and the T transformation.

polynomials over Γ_p, and functions of the form (6) over Γ_R. These "transfinite elements" thus ensure C^0 continuity across Γ_p and Γ_R as well as between adjacent elements of Ω_p. In the following, the trial functions are derived for the elements in Ω_p for the case in which Ω_0 is covered by linear isoparametric elements in the neighborhood of the singular point. As we wish to calculate the stiffness matrix $a_p(v,v)$ in terms of the standard coordinates (ξ,η), we will express the trial function over an element of Ω_p in terms of these coordinates. Referring to Fig. 3, the edge AB $(\eta = 0, 0 \leqslant \xi \leqslant 1)$ is mapped onto the circular arc $r = R$, $\beta_1 \leqslant \theta \leqslant \beta_2$, so that θ is a function of ξ only, and the function $f_i(r,\theta,\alpha_i)$ becomes $f_i(R,\theta,\alpha_i) = g(\xi,\alpha_i)$, say.

Let us first consider bilinear elements over Ω_0. Over the edges bc, cd, da we will take trial functions that interpolate linearly between the values at the vertices over each of these three edges. Since the bilinear blending transformation, and hence its inverse, will be linear over each of these edges, the trial function over the edges BC, CD, DA will also be a linear interpolant between the values at the vertices. Thus, if we denote by u_{11}, and u_{01} the nodal values of the trial functions at C and D, respectively, we have

$$u(\xi,0) = \sum_{i=1}^{N} A_i g_i(\xi,\alpha_i),$$

$$u(\xi,1) = u_{11} + (1-\xi)u_{01},$$

$$u(0,\eta) = (1-\eta)\sum_{i=1}^{N} A_i g_i(0,\alpha_i),$$

$$u(1,\eta) = (1-\eta)\sum_{i=1}^{N} A_i g_i(1,\alpha_i),$$

and the *linear blended trial function* for a typical element in Ω_p becomes

$$u_l(\xi,\eta) = (1-\eta)\sum_{i=1}^{N} A_i g_i(\xi,\alpha_i) + \eta[u_{01}(1-\xi) + u_{11}\xi]. \tag{10}$$

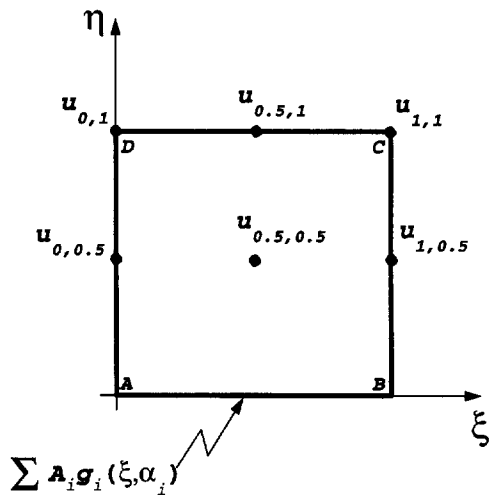

Fig. 4. Standard element corresponding to a quadratic element in Ω_p.

If biquadratic elements are being used over Ω_O, we take the trial function to be quadratic in ξ over the edge CD in the standard plane. As the intermediate node is at the mid-point of CD and T is linear, the intermediate node on cd will also be at its midpoint, and C^0 conformity will be maintained over cd, i.e. between Ω_p and Ω_O. The nodal values for the trial function for the element in the standard space (the quadratic case) are shown in Fig. 4. The *quadratic blended trial function*, is defined by

$$\begin{aligned}
u_q(\xi,\eta) &= (2\xi-1)(\xi-1)u(0,\eta) + 4\xi(1-\xi)u(0.5,\eta) + \xi(2\xi-1)u(1,\eta)\\
&\quad + (2\eta-1)(\eta-1)u(\xi,0) + 4\eta(1-\eta)u(\xi,0.5) + \eta(2\eta-1)u(\xi,1)\\
&\quad - [(2\xi-1)(\xi-1)(2\eta-1)(\eta-1)u(0,0) + 4(2\xi-1)(\xi-1)\eta(1-\eta)u(0,0.5)\\
&\quad + (2\xi-1)(\xi-1)\eta(2\eta-1)u(0,1) + 4\xi(1-\xi)(2\eta-1)(\eta-1)u(0.5,0)\\
&\quad + 16\xi(1-\xi)\eta(1-\eta)u(0.5,0.5) + 4\xi(1-\xi)\eta(2\eta-1)u(0.5,1)\\
&\quad + \xi(2\xi-1)(2\eta-1)(\eta-1)u(1,0) + 4\xi(1-\xi)\eta(1-\eta)u(1,0.5)\\
&\quad + \xi(2\xi-1)\eta(2\eta-1)u(1,1)].
\end{aligned}$$

Taking $u(\xi,0) = \sum_{i=1}^{N} A_i g_i(\xi,\alpha_i)$, $u(\xi,0.5)$ to be the unique quadratic function determined by the values of $u(0,0.5)$, $u(0.5,0.5)$, $u(1,0.5)$ and similarly for $u(\xi,1)$, $u(0,\eta)$, $u(0.5,\eta)$ and $u(1,\eta)$ we obtain

$$\begin{aligned}
u_q(\xi,\eta) &= (2\eta^2-3\eta+1)\sum_{i=1}^{N} A_i g_i(\xi,\alpha_i)\\
&\quad + [u_{0,0.5}(2\xi^2-3\xi+1) + u_{0.5,0.5}(-4\xi^2+4\xi) + u_{1,0.5}(2\xi^2-\xi)](-4\eta^2+4\eta)\\
&\quad + [u_{0,1}(2\xi^2-3\xi+1) + u_{0.5,1}(-4\xi^2+4\xi) + u_{1,1}(2\xi^2-\xi)](2\eta^2-\eta). \qquad (11)
\end{aligned}$$

One could use a biquadratic blending transformation instead of a bilinear one. However, experiments with a simple elastostatic problem (the first problem in [10]), showed that this results in only a marginal improvement in the results, and is not worth the algebraic and computational effort involved.

The Jacobian of the transformation is

$$J = \det\left(\frac{\partial(r,\theta)}{\partial(\xi,\eta)}\right), \tag{12}$$

so that the derivatives of the trial functions can be computed in the standard space using (9) and (12):

$$\begin{aligned}\frac{\partial u}{\partial r} &= \frac{1}{J}\left[\frac{\partial u}{\partial \xi}\frac{\partial \theta}{\partial \eta} - \frac{\partial u}{\partial \eta}\frac{\partial \theta}{\partial \xi}\right],\\ \frac{\partial u}{\partial \theta} &= \frac{1}{J}\left[-\frac{\partial u}{\partial \xi}\frac{\partial r}{\partial \eta} + \frac{\partial u}{\partial \eta}\frac{\partial r}{\partial \xi}\right].\end{aligned} \tag{13}$$

Substituting (13) into the bilinear form of (4), we obtain the contribution to $a_p(v,v)$ from a single element of Ω_p:

$$\int_0^1\int_0^1 \frac{1}{J}\left\{\left(\frac{\partial u}{\partial \xi}\right)^2\left[\left(\frac{\partial \theta}{\partial \eta}\right)^2 + \frac{1}{r^2}\left(\frac{\partial r}{\partial \eta}\right)^2\right] + \left(\frac{\partial u}{\partial \eta}\right)^2\left[\left(\frac{\partial \theta}{\partial \xi}\right)^2 + \frac{1}{r^2}\left(\frac{\partial r}{\partial \xi}\right)^2\right] - 2\frac{\partial u}{\partial \xi}\frac{\partial u}{\partial \eta}\left[\frac{\partial \theta}{\partial \xi}\frac{\partial \theta}{\partial \eta} + \frac{1}{r^2}\frac{\partial r}{\partial \xi}\frac{\partial r}{\partial \eta}\right]\right\} \mathrm{d}\xi\,\mathrm{d}\eta. \tag{14}$$

The stiffness matrix for the whole domain Ω_p is obtained once (10) (or (11) if quadratic elements are used) and (12) are substituted into (14) and the contributions from all the elements of Ω_p summed up by the usual assembly procedure. The bilinear form $a_p(u,u)$ has as unknowns the N coefficients of the asymptotic expansion (A_i) as well as the nodal values on the polygon Γ_p and other internal nodal values $(u_{0,0.5}, u_{0.5,0.5}, \ldots)$.

The SSE stiffness matrix will be obtained by combining the stiffness matrices corresponding to $a_R(u,u)$ and $a_p(u,u)$, and hence will be based on two types of degrees of freedom: the nodal values laying on Γ_p, which are common to the SSE and the outer domain Ω_O, and the coefficients of the asymptotic expansion and some internal nodal values which are not common to Ω_O. As the latter represent internal degrees of freedom, they can be eliminated by static condensation, leaving a stiffness matrix for the SSE in terms of the nodal values laying on Γ_p alone. We also store an auxiliary matrix, which is used at the end of the calculation to recover the coefficients of the asymptotic expansion (A_i).

The formulation of the SSE bilinear form for the elastostatic problem is analogous to the scalar elliptic problem, except for being more complicated due to existence of two displacement fields. Explicit expressions for $a_R(\boldsymbol{u},\boldsymbol{u})$ and $a_p(\boldsymbol{u},\boldsymbol{u})$ for the elastostatic problem are given in Appendix A.

Once the stiffness matrix is computed for the SSE, it can by assembled into the global stiffness matrix for the outer domain Ω_O. In fact, for the scalar and elastostatic problems, the total stiffness matrix dimension remains unchanged because the condensed SSE stiffness matrix contains nodal values corresponding to the polygon Γ_p only. The resulting global stiffness matrix remains symmetric,

and only slightly more populated due to the connections between the degrees of freedom on the polygon Γ_p. The system of equations is solved by Gaussian elimination with pivotting.

3. Numerical examples

We illustrate the method on three problems for which previous results are available. Two of them concern Laplace's equation, the singularity being caused by an abrupt change in the specified boundary conditions in the first case, and by a reentrant corner on the boundary in the second. The third is an elastostatic problem, in which the presence of a crack results in a reentrant corner on the domain boundary. These problems were chosen because, in each case, the domain has a simple form which has enabled results of high accuracy to be obtained using a variety of methods which are of less general applicability than the current scheme. We will, therefore, take these results as benchmarks against which the accuracy of the current results may be assessed. The application of the present scheme to more difficult geometries has been illustrated for the elastostatic case in [10], some of the problems treated requiring superelements of more general shape than the rectangles used herein.

3.1. The "Motz Problem" – Laplace's equation

We consider the solution of Laplace's equation over the region $-1 < x < 1$, $0 < y < 1$ shown in Fig. 5 subject to the boundary conditions

$$u = \begin{cases} 0 & \text{on } -1 \leqslant x \leqslant 0,\ y = 0, \\ 500 & \text{on } x = 1,\ 0 \leqslant y \leqslant 1, \end{cases} \qquad \partial u/\partial n = 0 \quad \text{elsewhere on the boundary.} \tag{15}$$

The discontinuity at the origin in the boundary conditions along the line $y = 0$ results in a singularity at this point. The asymptotic expansion of the solution about the origin is of the form [14]

$$u = \sum_{n=0}^{\infty} c_n r^{n+1/2} \cos[(n + \tfrac{1}{2})\theta]. \tag{16}$$

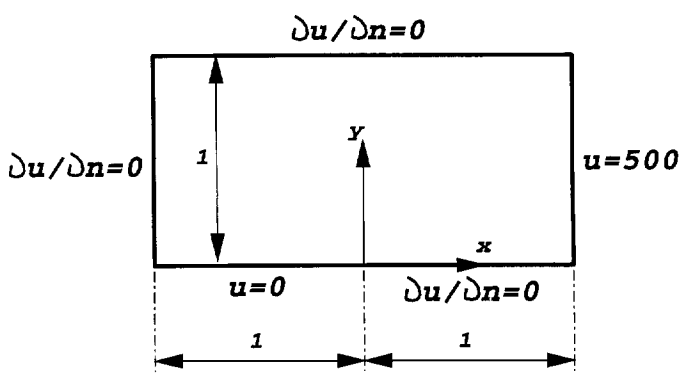

Fig. 5. Domain and boundary conditions for the Motz problem.

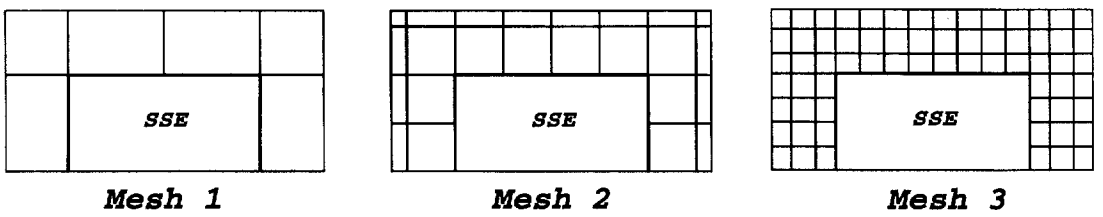

Fig. 6. Meshes used for the Motz problem.

This problem was first formulated by Motz [14] in a slightly different form. He solved it by finite differences, modifying the usual finite difference approximation in the neighborhood of the singularity so as to take into account the form of the asymptotic expansion for the solution. The Motz problem has served as a simple test case for many methods of dealing with singularities in elliptic boundary problems, among them expansion in dual series [15], conversion to a boundary integral equation [16], conformal transformation to a simpler domain [17], and determination of the coefficients in the asymptotic expansion (16) by least-squares fitting of the boundary conditions [18].

Accurate solutions have been obtained by various authors over a grid of points of size $h = \frac{2}{7}$ in both directions, and over a grid of size $h = \frac{1}{28}$ over the region $|x| \leqslant \frac{1}{7}$, $0 \leqslant y \leqslant \frac{1}{7}$. We shall refer to these as the coarse and fine grids, respectively. The current method was applied over several different finite element meshes which are illustrated in Fig. 6.

Six terms were included in the truncated series (16), and the superelement occupied the region $|x| \leqslant \frac{4}{7}$, $0 \leqslant y \leqslant \frac{4}{7}$ with $R = 0.9 \times \frac{4}{7}$ (see Section 3.4). Ordinary Gaussian quadrature is adequate for evaluating the integrals (7), as only non-negative integral powers of r appear in the integrand. The mesh was designed in each case so as to facilitate the computation of the solution at the points of the above-mentioned coarse grid. Our values over these grids were obtained in the following manner. For points inside the superelement we evaluated the truncated series (16) using the values of the coefficients given by the solution program. For points outside the superelement or on its boundary, we used the nodal values from the solution, making use of the appropriate finite element interpolant if the grid point did not coincide with one of our nodes. In order to assess the accuracy of our results we will take the results obtained by the conformal transformation method of Whiteman and Papamichael [17] as being exact. Levin and Sideridis[2] have computed this case over the coarse grid by the method of [17] and also by boundary collocation. Their results, listed to three figures after the decimal point, agree with one another and also with those given by the Li et al. series [18], obtained by least-squares fitting over the boundary, to within a maximum difference of 0.006. This excellent agreement makes this problem a very good benchmark. The conformal transformation results [17] over the fine grid are given to two digits after the decimal point, and agree to within a maximum difference of 0.02 with the extended dual series results of Whiteman [15], and the values obtained from the Li et al. series. In fact, the results of the three calculations agree to all the figures given at nearly all of the points of the fine grid.

[2] D. Levin and A. Sideridis, A collocation technique for certain singular harmonic mixed boundary value problems, Technical Report TR/73, Department of Mathematics, Brunel University, 1977 (unpublished).

Table 1
Maximum error at the grid points for the Motz problem

Elements used	No. of external d.o.f.	Total no. of d.o.f.	Maximum error	Maximum relative error
Quadratic, mesh 2	101	124	0.065	0.00013
Quadratic, mesh 1	33	47	0.39	0.0008
Linear, mesh 3	92	98	0.55	0.0011
Linear, mesh 2	39	45	1.83	0.0037

Table 2
Values for the series coefficients c_n for the Motz problem

n	Li et al. [18]	Quadratic mesh 2	Quadratic mesh 1	Linear mesh 3	Linear mesh 2
0	401.162	401.166	401.202	401.379	401.605
1	87.656	87.657	87.677	87.605	87.614
2	17.238	17.236	17.366	17.143	16.670
3	−8.071	−8.061	−7.690	−8.719	−7.133
4	1.440	1.432	2.741	−1.481	−2.886
5	0.331	0.570	1.758	1.588	1.297

In Table 1 we list the maximum over all points of the two grids of the difference between the "exact" results and those of the current method (this maximum always occurred at a point of the coarse grid) and later we will refer to the accuracy of the series coefficients c_i, which determine the accuracy of the solution near the singular point. The maximum relative error is defined by $(u^{FE} - u^{EX})/u^{EX}_{max}$, where u^{EX}_{max} in the domain is 500. The number of degrees of freedom (d.o.f.) is the number of nodal values in Ω_o, including those on the boundary of the superelement, and gives the size of the set of linear equations to be solved. The total number of d.o.f. includes the internal nodes of the superelement (in the quadratic case) and the series coefficients, both of which can be recovered from the solution with the aid of the auxiliary matrix referred to in Section 2.

We see from the results listed that a quadratic element yields errors of an order of magnitude smaller than a linear one for a given number of d.o.f. In Table 2 we list the values of the series coefficients obtained using each of the four meshes, compared with those of Li et al. [18]. The first three coefficients are obtained with good accuracy, and the improvement in accuracy as the number of d.o.f. is increased or, as quadratic elements are used instead of linear ones, is more marked than the improvement in the solution itself.

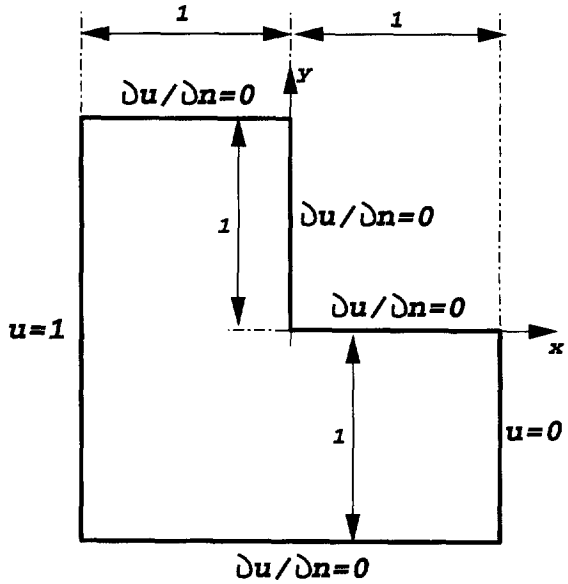

Fig. 7. L-shaped domain and boundary conditions.

3.2. Laplace's equation over an L-shaped domain

The domain is illustrated in Fig. 7. The boundary conditions are the following:

$$\begin{array}{ll} u = 1 & \text{on } x = -1,\ -1 \leqslant y \leqslant 1, \\ u = 0 & \text{on } x = 1,\ -1 \leqslant y \leqslant 0, \\ \partial u/\partial n = 0 & \text{elsewhere on the boundary.} \end{array} \tag{17}$$

The singularity arises from the reentrant corner of magnitude $3\pi/2$ at the origin. The asymptotic expansion for the solution about the origin is of the form

$$u = \sum_{n=0}^{\infty} c_n r^{2n/3} \cos[(2n/3)\theta], -3\pi/2 \leqslant \theta \leqslant 0. \tag{18}$$

Computations were carried out using a mesh of quadratic rectangular elements with a quadratic superelement around the singularity, and a linear mesh with a linear superelement, as shown in Fig. 8. In each case, the superelement covered the part of the domain for which $|x|, |y| \leqslant 0.6$, and four terms were included in the series (18). Computations have also been made for this problem by several authors using integral equation [16] or conformal transformation [19] methods, the results being listed over a grid of size 0.2×0.2. The results obtained by the three methods agree with one another to within a maximum difference of 0.0002. The collocation results are given to six figures after the decimal point, and we will treat them as exact, and use them to determine the error in our computed values at the points of this grid, our values at the grid points being computed in a manner analogous to that used in the case of Problem 1. The results are summarized in Table 3. The error listed is the largest error at a grid point. As the maximum value of the solution is $u = 1.0$, the relative and absolute errors are identical. For this problem, the accuracy of the numerical quadrature

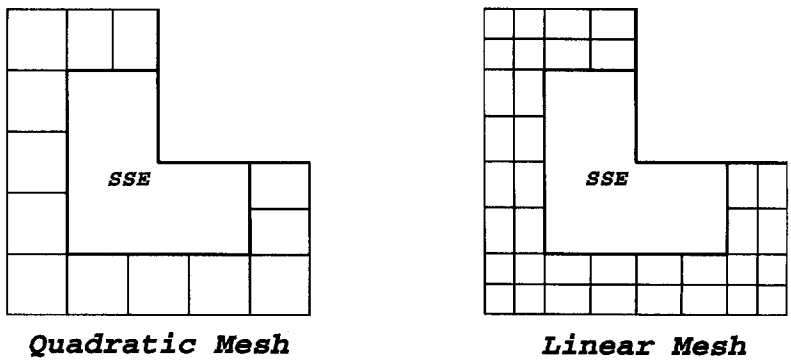

Fig. 8. Meshes used for the L-shaped domain.

Table 3
Maximum error at the grid points for the L-shaped domain

Elements used	No. of external d.o.f.	Total no. of d.o.f.	Maximum error
Quadratic mesh	68	99	0.0002
Linear mesh	57	67	0.0015

Table 4
Values for the series coefficients c_n for the L-shaped domain

n	Quadratic mesh	Linear mesh
0	0.6667	0.6667
1	−0.4520	−0.4527
2	−0.2149	−0.2142
3	0.0000	0.0000

was checked by computing the SSE also using the adaptive scheme. The values of the solution and the series coefficients obtained using the two schemes differed by at most 0.0001. We list our values for the series coefficients for reference in Table 4 (the first series coefficient is the well known "flux intensity factor"). We are not aware of any other calculations of these coefficients with which the current results could be compared.

3.3. Central crack in a rectangular plate – elastostatic problem

To demonstrate the accuracy, efficiency and ease of application of the method, a sample central crack problem in a rectangular plate subjected to tension has been treated using the SSE, and the results compared with the analytic result. We assume the material is homogeneous, isotropic and linearly elastic.

With the usual assumptions of linear elasticity, the asymptotic series (6) can be represented as follows [20]:

$$\begin{aligned} u_1 = (u_1)_0 + \frac{1}{2\mu}\sum_{i=1}^{\infty} & A_i r^{(i-1/2)}[(\kappa + i - \tfrac{3}{2})\cos(i - \tfrac{1}{2})\theta - (i - \tfrac{1}{2})\cos(i - \tfrac{5}{2})\theta] \\ & + B_i r^{(i-1/2)}[-(\kappa + i + \tfrac{1}{2})\sin(i - \tfrac{1}{2})\theta + (i - \tfrac{1}{2})\sin(i - \tfrac{5}{2})\theta] \\ & + C_i r^{i}[(\kappa + i + 1)\cos(i\theta) - i\cos(i - 2)\theta] \\ & + D_i r^{i}[-(\kappa + i - 1)\sin(i\theta) + i\sin(i - 2)\theta] \end{aligned} \tag{19}$$

and

$$\begin{aligned} u_2 = (u_2)_0 + \frac{1}{2\mu}\sum_{i=1}^{\infty} & A_i r^{(i-1/2)}[(\kappa - i - \tfrac{3}{2})\sin(i - \tfrac{1}{2})\theta + (i - \tfrac{1}{2})\sin(i - \tfrac{5}{2})\theta] \\ & + B_i r^{(i-1/2)}[(\kappa - i - \tfrac{1}{2})\cos(i - \tfrac{1}{2})\theta + (i - \tfrac{1}{2})\cos(i - \tfrac{5}{2})\theta] \\ & + C_i r^{i}[(\kappa - i - 1)\sin(i\theta) + i\sin(i - 2)\theta] \\ & + D_i r^{i}[(\kappa - i + 1)\cos(i\theta) + i\cos(i - 2)\theta], \end{aligned} \tag{20}$$

where $((u_1)_0, (u_2)_0)$ denotes (u_1, u_2) at $r = 0$, and κ and μ are defined in Appendix A. If the symmetry and loading conditions are such that only mode 1 displacements occur, then $B_i = D_i = 0$ for all i, while for mode 2 displacements, $A_i = C_i = 0$ for all i. The stress intensity factors K_{I} and K_{II} for modes 1 and 2, respectively, are given in terms of the coefficients of the series (19) and (20) by

$$K_{\mathrm{I}} = A_1\sqrt{2\pi} \quad \text{and} \quad K_{\mathrm{II}} = -B_1\sqrt{2\pi}.$$

As a result of symmetry, one-quarter of the plate containing the central crack is considered. A coarse and a refined mesh were considered as shown in Fig. 9. The dimensions of the plate are $a/b = 0.5$, and $h/b = 1.0$, and quadratic isoparametric shape functions were used. The following values for the essential parameters are assumed: Poisson's ratio $\nu = 0.33$, Young's modulus $E = 1.0$, uniform tension $\sigma_y = 1$, and plane stress situation. For this geometry, the non-dimensional stress intensity factor given by Isida [21] is 1.334; this result is said to be exact to four significant figures. We obtain the value of 1.3323 with the coarse mesh, and 1.3339 with the refined mesh shown, using 16 terms in the expansion, and with a value of 0.4 for R/a.

The results show that the present method yields accurate results for the stress intensity factor using coarse meshes. Further examples for the use of the SSE to obtain the coefficients of the asymptotic expansion for crack and V-notch problems, including mixed mode, and slanted cracks can be found in [10].

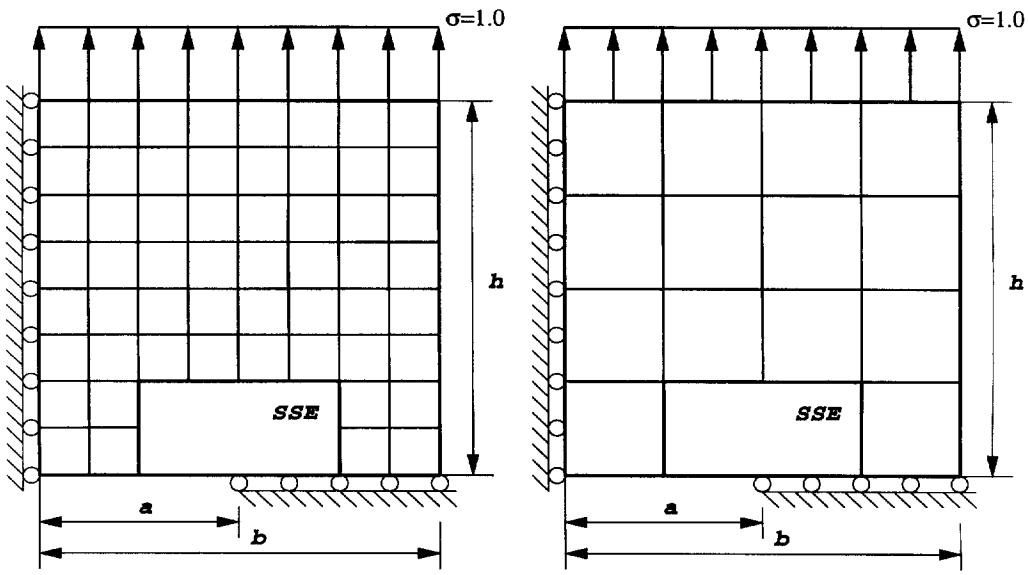

Fig. 9. Elastostatic crack problem: domain, boundary conditions and meshes employed.

3.4. Dependence of the results on the superelement parameters

Let $2l$ denote the length of the longest side of the superelement. For a superelement with given geometry, the parameters to be chosen are the ratio R/l of the radius of the circular region to the size of the superelement, and the number N of terms to be included in the truncated series (6).

For the Laplace equation (Problems 1 and 2), the maximum error is found to be comparatively insensitive to the value of R/l in the range 0.6–0.9, and in particular for values between 0.75 and 0.9. For the Motz case, where the "exact" values of the series coefficients are known, the best results for the coefficients were obtained using a value of 0.9 for R/l. We adopted this value, therefore, for the two problems. As regards the value of N, we took N to be 6 for the Motz problem, and 4 for the L-shaped domain. The inclusion of a larger number of terms led to no improvement, the accuracy remaining unchanged.

For the elastostatic problem, the result of main interest is the non-dimensional stress intensity factor, the "exact" value being 1.334, as quoted above. The current method gives the values of 1.3176, 1.3322, 1.3323 and 1.3323 for the coarse mesh, and 1.3195, 1.3338, 1.3339 and 1.3339 for the refined mesh for $N=8$, 12, and 16 or 20 respectively with a value of 0.8 for R/l. As regards the dependence on R/l, with $N=16$, we obtain 1.3344 for $R/l = 0.5$, 1.3340 for $R/l = 0.6$, and 1.3339 for R/l in the range 0.7 to 0.9 using the refined mesh. Again, the result is insensitive to the value of R/l in this range.

It should be noted that the optimal size for the SSE is problem-dependent. If the asymptotic series coefficients turn out to be relatively large, then the SSE should be correspondingly large, in order to avoid loss of accuracy. For a problem with a complicated geometry, it may be necessary to choose the size of the SSE adaptively. This could increase the complexity of the method. On the other hand,

such a problem would in any case require a certain amount of adaptivity in choosing the mesh over the whole domain.

The results for all three problems indicate that accurate values for the solution and for the series coefficients can be obtained using the quadratic superelement with quite a coarse mesh. Indeed, the results for the fine mesh were computed mainly to show what is the ultimate accuracy which can be achieved, the results from the coarse meshes being sufficient for all practical purposes.

4. Conclusions

Superelements incorporating blending functions have been designed to enable the finite element schemes to deal with the difficulties caused by singularities in the solution of two-dimensional elliptic boundary value problems arising from abrupt changes in the boundary conditions or in the direction of the boundary. Application to benchmark problems for the Laplace equation and to linear elasticity show the method to be both accurate and efficient. The computation yields values for the coefficients in the asymptotic series representing the solution in the vicinity of the singular point, as well as for the solution over the rest of the domain. The leading coefficients, which are obtained with high accuracy, are of particular practical importance in many cases, e.g. the stress intensity factors for linear elasticity, for which excellent results have been obtained for a variety of cases [10]. The superelements may be incorporated into standard commercial finite element codes, as described in [11]. The use of the SSE has the following advantages over other methods which have been suggested:

(a) The coefficients of the series are obtained directly from the computation with high accuracy and efficiency.

(b) The SSE can be a convex polygon of any shape, and is easily incorporated in many commercial finite element codes.

(c) Any singular displacement field of known form may be represented by the SSE in a similar manner to those discussed herein.

(d) For a given number of degrees of freedom the SSE provides higher accuracy when compared with many other elements (see comparison to other methods for the computation of stress intensity factors in [10]).

The method may be extended to elliptic problems involving other types of singularities, such as those caused by an interface between two different elastic materials for example, provided that the form of the asymptotic series for the solution in the vicinity of the singular point is known. In some cases, the eigenfunctions $f_i(r, \theta, \alpha_i)$ can not always be computed explicitly, and numerical approximations to f_i and α_i (see e.g. [22] and references therein) have to be used. The use of these approximate values will affect the accuracy of the extracted coefficients, and detailed numerical and mathematical analysis, beyond of the scope of this paper, would need to be performed in order to assess the overall accuracy achieved in such cases.

The SSE method has been extended to compute eigenvalues for the Laplacian over two-dimensional domains with reentrant corners, and applied to determine cut-off frequencies for an electromagnetic waveguide, in the manner of [23], the preliminary results being promising.

Acknowledgements

The authors are grateful to Professors Michel Bercovier, Barna A. Szabó, Benqi Guo and Soren Jensen for helpful comments and suggestions on the manuscript.

Appendix A. SSE bilinear forms for the elastostatic problem

Denote the displacement vector by $\boldsymbol{u} = (u_1, u_2)^{\mathrm{T}}$. In the vicinity of the singular point

$$\boldsymbol{u} = \sum_i A_i \left(f_{1i}(r,\theta,\alpha_i)\ f_{2i}(r,\theta,\alpha_i)\right)^{\mathrm{T}}.$$

Using the space spanned by above $\boldsymbol{u}$ for the trial space, the bilinear form in Ω_R is obtained:

$$\begin{aligned} a_R(\boldsymbol{u},\boldsymbol{u}) = \int_0^R \int_{-\pi+\gamma/2}^{\pi-\gamma/2} \Bigg\{ & c_1 \left[\left(\cos\theta \frac{\partial u_1}{\partial r} - \frac{\sin\theta}{r}\frac{\partial u_1}{\partial \theta} \right)^2 + \left(\sin\theta \frac{\partial u_2}{\partial r} + \frac{\cos\theta}{r}\frac{\partial u_2}{\partial \theta} \right)^2 \right] \\ & + c_2 \left(\sin\theta \frac{\partial u_2}{\partial r} + \frac{\cos\theta}{r}\frac{\partial u_2}{\partial \theta} \right) \left(\cos\theta \frac{\partial u_1}{\partial r} - \frac{\sin\theta}{r}\frac{\partial u_1}{\partial \theta} \right) \\ & + c_3 \left(\sin\theta \frac{\partial u_1}{\partial r} + \frac{\cos\theta}{r}\frac{\partial u_1}{\partial \theta} + \cos\theta \frac{\partial u_2}{\partial r} - \frac{\sin\theta}{r}\frac{\partial u_2}{\partial \theta} \right)^2 \Bigg\} r\, dr\, d\theta, \end{aligned}$$

$$c_1 = \mu \frac{\kappa+1}{\kappa-1}, \qquad c_2 = 2\mu \frac{3-\kappa}{\kappa-1}, \qquad c_3 = \mu,$$

$$\mu = \frac{E}{2(1+\nu)}, \qquad \kappa = \begin{cases} (3-\nu)/(1+\nu), & \text{plane stress}, \\ 3-4\nu, & \text{plane strain}, \end{cases}$$

E is Young's modulus and ν Poisson's ratio. The expression for the bilinear form $a_p(\boldsymbol{u},\boldsymbol{u})$ where $u_{,\xi}$ stands for $\partial u/\partial\xi$ and $u_{,\eta}$ stands for $\partial u/\partial\eta$ (over Ω_p) is given by

$$\begin{aligned} \int_0^1 \int_0^1 \Bigg[\Bigg[& u_{1,\xi}^2 \left\{ \frac{c_1 r}{J} \left[\cos^2\theta \left(\frac{\partial\theta}{\partial\eta}\right)^2 + \frac{\sin 2\theta}{r} \left(\frac{\partial\theta}{\partial\eta}\frac{\partial r}{\partial\eta}\right) + \frac{\sin^2\theta}{r^2}\left(\frac{\partial r}{\partial\eta}\right)^2 \right] \right. \\ & \left. + \frac{c_3 r}{J} \left[\sin^2\theta \left(\frac{\partial\theta}{\partial\eta}\right)^2 - \frac{\sin 2\theta}{r} \left(\frac{\partial\theta}{\partial\eta}\frac{\partial r}{\partial\eta}\right) - \frac{\cos^2\theta}{r^2}\left(\frac{\partial r}{\partial\eta}\right)^2 \right] \right\} \\ & + u_{1,\eta}^2 \left\{ \frac{c_1 r}{J} \left[\cos^2\theta \left(\frac{\partial\theta}{\partial\xi}\right)^2 + \frac{\sin 2\theta}{r} \left(\frac{\partial\theta}{\partial\xi}\frac{\partial r}{\partial\xi}\right) + \frac{\sin^2\theta}{r^2}\left(\frac{\partial r}{\partial\xi}\right)^2 \right] \right. \\ & \left. + \frac{c_3 r}{J} \left[\sin^2\theta \left(\frac{\partial\theta}{\partial\xi}\right)^2 - \frac{\sin 2\theta}{r} \left(\frac{\partial\theta}{\partial\xi}\frac{\partial r}{\partial\xi}\right) + \frac{\cos^2\theta}{r^2}\left(\frac{\partial r}{\partial\xi}\right)^2 \right] \right\} \\ & + u_{2,\xi}^2 \left\{ \frac{c_1 r}{J} \left[\sin^2\theta \left(\frac{\partial\theta}{\partial\eta}\right)^2 - \frac{\sin 2\theta}{r} \left(\frac{\partial\theta}{\partial\eta}\frac{\partial r}{\partial\eta}\right) + \frac{\cos^2\theta}{r^2}\left(\frac{\partial r}{\partial\eta}\right)^2 \right] \right. \\ & \left. + \frac{c_3 r}{J} \left[\cos^2\theta \left(\frac{\partial\theta}{\partial\eta}\right)^2 + \frac{\sin 2\theta}{r} \left(\frac{\partial\theta}{\partial\eta}\frac{\partial r}{\partial\eta}\right) + \frac{\sin^2\theta}{r^2}\left(\frac{\partial r}{\partial\eta}\right)^2 \right] \right\} \end{aligned}$$

$$+u_{2,\eta}^2\left\{\frac{c_1 r}{J}\left[\sin^2\theta\left(\frac{\partial\theta}{\partial\xi}\right)^2-\frac{\sin 2\theta}{r}\left(\frac{\partial\theta}{\partial\xi}\frac{\partial r}{\partial\xi}\right)+\frac{\cos^2\theta}{r^2}\left(\frac{\partial r}{\partial\xi}\right)^2\right]\right.$$

$$\left.+\frac{c_3 r}{J}\left[\cos^2\theta\left(\frac{\partial\theta}{\partial\xi}\right)^2+\frac{\sin 2\theta}{r}\left(\frac{\partial\theta}{\partial\xi}\frac{\partial r}{\partial\xi}\right)+\frac{\sin^2\theta}{r^2}\left(\frac{\partial r}{\partial\xi}\right)^2\right]\right\}$$

$$+2u_{1,\xi}u_{1,\eta}\left\{\frac{c_1 r}{J}\left[-\cos^2\theta\left(\frac{\partial\theta}{\partial\eta}\frac{\partial\theta}{\partial\xi}\right)-\frac{\sin 2\theta}{2r}\left(\frac{\partial\theta}{\partial\eta}\frac{\partial r}{\partial\xi}\right)\right.\right.$$

$$\left.-\frac{\sin 2\theta}{2r}\left(\frac{\partial r}{\partial\eta}\frac{\partial\theta}{\partial\xi}\right)-\frac{\sin^2\theta}{r^2}\left(\frac{\partial r}{\partial\eta}\frac{\partial r}{\partial\xi}\right)\right]$$

$$+\frac{c_3 r}{J}\left[-\sin^2\theta\left(\frac{\partial\theta}{\partial\eta}\frac{\partial\theta}{\partial\xi}\right)+\frac{\sin 2\theta}{2r}\left(\frac{\partial\theta}{\partial\eta}\frac{\partial r}{\partial\xi}\right)\right.$$

$$\left.\left.+\frac{\sin 2\theta}{2r}\left(\frac{\partial r}{\partial\eta}\frac{\partial\theta}{\partial\xi}\right)-\frac{\cos^2\theta}{r^2}\left(\frac{\partial r}{\partial\eta}\frac{\partial r}{\partial\xi}\right)\right]\right\}$$

$$+2u_{2,\xi}u_{2,\eta}\left\{\frac{c_1 r}{J}\left[-\sin^2\theta\left(\frac{\partial\theta}{\partial\eta}\frac{\partial\theta}{\partial\xi}\right)+\frac{\sin 2\theta}{2r}\left(\frac{\partial\theta}{\partial\eta}\frac{\partial r}{\partial\xi}\right)\right.\right.$$

$$\left.+\frac{\sin 2\theta}{2r}\left(\frac{\partial r}{\partial\eta}\frac{\partial\theta}{\partial\xi}\right)-\frac{\cos^2\theta}{r^2}\left(\frac{\partial r}{\partial\eta}\frac{\partial r}{\partial\xi}\right)\right]$$

$$+\frac{c_3 r}{J}\left[-\cos^2\theta\left(\frac{\partial\theta}{\partial\eta}\frac{\partial\theta}{\partial\xi}\right)-\frac{\sin 2\theta}{2r}\left(\frac{\partial\theta}{\partial\eta}\frac{\partial r}{\partial\xi}\right)\right.$$

$$\left.\left.-\frac{\sin 2\theta}{2r}\left(\frac{\partial r}{\partial\eta}\frac{\partial\theta}{\partial\xi}\right)-\frac{\sin^2\theta}{r^2}\left(\frac{\partial r}{\partial\eta}\frac{\partial r}{\partial\xi}\right)\right]\right\}$$

$$+2u_{1,\xi}u_{2,\xi}\left\{\left[\frac{c_3 r}{J}+\frac{c_2 r}{2J}\right]\right.$$

$$\left.\left[\frac{\sin 2\theta}{2}\left(\frac{\partial\theta}{\partial\eta}\right)^2+\frac{\sin^2\theta}{r}\left(\frac{\partial\theta}{\partial\eta}\frac{\partial r}{\partial\eta}\right)-\frac{\cos^2\theta}{r}\left(\frac{\partial\theta}{\partial\eta}\frac{\partial r}{\partial\eta}\right)-\frac{\sin 2\theta}{2r^2}\left(\frac{\partial r}{\partial\eta}\right)^2\right]\right\}$$

$$+2u_{1,\eta}u_{2,\eta}\left\{\left[\frac{c_3 r}{J}+\frac{c_2 r}{2J}\right]\right.$$

$$\left.\left[\frac{\sin 2\theta}{2}\left(\frac{\partial\theta}{\partial\xi}\right)^2+\frac{\sin^2\theta}{r}\left(\frac{\partial\theta}{\partial\xi}\frac{\partial r}{\partial\xi}\right)-\frac{\cos^2\theta}{r}\left(\frac{\partial\theta}{\partial\xi}\frac{\partial r}{\partial\xi}\right)-\frac{\sin 2\theta}{2r^2}\left(\frac{\partial r}{\partial\xi}\right)^2\right]\right\}$$

$$+2u_{1,\xi}u_{2,\eta}\left\{\left[\frac{c_3 r}{J}+\frac{c_2 r}{2J}\right]\left[-\frac{\sin 2\theta}{2}\left(\frac{\partial\theta}{\partial\eta}\frac{\partial\theta}{\partial\xi}\right)-\frac{\sin^2\theta}{r}\left(\frac{\partial\theta}{\partial\eta}\frac{\partial r}{\partial\xi}\right)+\frac{\cos^2\theta}{r}\left(\frac{\partial r}{\partial\eta}\frac{\partial\theta}{\partial\xi}\right)+\frac{\sin 2\theta}{2r^2}\left(\frac{\partial r}{\partial\eta}\frac{\partial r}{\partial\xi}\right)\right]\right\}$$

$$+2u_{1,\eta}u_{2,\xi}\left\{\left[\frac{c_3 r}{J}+\frac{c_2 r}{2J}\right]\left[-\frac{\sin 2\theta}{2}\left(\frac{\partial\theta}{\partial\eta}\frac{\partial\theta}{\partial\xi}\right)-\frac{\sin^2\theta}{r}\left(\frac{\partial r}{\partial\eta}\frac{\partial r}{\partial\xi}\right)+\frac{\cos^2\theta}{r}\left(\frac{\partial\theta}{\partial\eta}\frac{\partial r}{\partial\xi}\right)+\frac{\sin 2\theta}{2r^2}\left(\frac{\partial r}{\partial\eta}\frac{\partial r}{\partial\xi}\right)\right]\right\}\Bigg]\mathrm{d}\xi\mathrm{d}\eta.$$

References

[1] J.T. Oden and J.N. Reddy, *Variational Methods in Theoretical Mechanics*, Springer, New York, NY, 1983.

[2] V.A. Kondratiev, "Boundary value problems for elliptic equations in domains with conical or angular points", *Trans. Moscow Math. Soc.* **16**, pp. 227–313, 1967.

[3] P. Grisvard, *Elliptic Problems in Nonsmooth Domains*, Pitman, England, 1985.

[4] I. Babuška and B.Q. Guo, The h, p and h–p version of the finite element method – basic theory and application, Technical note BN-1134, Institute for physical sciences and technology, university of Maryland at College Park, May 1992.

[5] G. Strang and G.J. Fix, *An Analysis of the Finite Element Method*, Prentice-Hall, Englewood cliffs, NJ, 1973.

[6] J.R. Whiteman and J.E. Akin, "Finite elements, singularities and fracture", in: J.R. Whiteman (ed.), *The Mathematics of Finite Elements and its Applications III*, Academic Press, London, pp. 35–54, 1979.

[7] S.N. Atluri and M. Nakagaki, "Computational methods for plane problems of fracture", in: S.N. Atluri (ed.), *Computational Methods in the Mechanics of Fracture*; Elsevier, Amsterdam, pp. 169–227, 1986.

[8] I. Babuška and H-S. Oh, "The p-version of the finite element method for domains with corners and for infinite domains", *Numer. Methods PDEs* **6**, pp. 371–392, 1990.

[9] G. Ogen and B. Schiff, "Constrained finite elements for singular boundary value problems", *J. Comp. Phys.* **51**, pp. 65–82, 1983.

[10] Z. Yosibash and B. Schiff, A superelement for two-dimensional singular boundary value problems in linear elasticity, *Int. J. Fract.* **62** (4), pp. 325–340, 1993.

[11] Z. Yosibash, D. Saltoun and B. Schiff, "An improved element to cover 2-D singular points arising from sharp edges and cracks – Element characteristics, experience and implementation via MSC/NASTRAN", in: *Proc. 19th MSC European user's Conf.*, Amsterdam, Holland, 1992.

[12] I.S. Sokolnikoff, *Mathematical Theory of Elasticity*, McGraw-Hill, New York, 1956.

[13] W.J. Gordon and C.A. Hall, "Transfinite element methods: blending functions interpolation over arbitrary curved element domains," *Numer. Math.* **21**, pp. 109–129, 1973.

[14] H. Motz, "The treatment of singularities of partial differential equations by relaxation methods", *Quart. Appl. Math.* **4**, p. 371, 1946.

[15] J.R. Whiteman, "Numerical solution of a harmonic mixed boundary value problem by the extension of a dual series method", *Quart. J. Mech. Appl. Math.* **23**, p. 449, 1970.

[16] G.T. Symm, Treatment of singularities in the solution of Laplace's equation by an integral equation method, Report NAC 31, National Physical Laboratory, 1973.

[17] J.R. Whiteman and N. Papamichael, "Treatment of harmonic mixed boundary value problems by conformal transformation methods", *Z. Angew. Math. Phys.* **23**, p. 655, 1972.

[18] Z-C. Li, R. Mathon and P. Sermer, "Boundary methods for solving elliptic problems with singularities and interfaces", *SIAM J. Numer. Anal.* **24**, p. 487, 1987.

[19] N. Papamichael and A. Sideridis, "The use of conformal transformations for the numerical solution of elliptic boundary value problems with boundary singularities", *J. Inst. Math. Appl.* **23**, p. 73, 1979.

[20] M.L. Williams, "On the stress distribution at the base of a stationary crack", *Trans. ASME J. Appl. Mech.* **24**, pp. 109–114, 1957.

[21] M. Isida, "Effect of width and length on stress intensity factors of internally cracked plates under various boundary conditions", *Int. J. Fracture Mech.* **7**, pp. 301–316, 1971.

[22] Z. Yosibash and B.A. Szabó, "Numerical analysis of singularities in two-dimensions. Part 1: Computation of eigenpairs", *Int. J. Numer. Meth. Eng.* **38** (12), pp. 2055–2082, 1995.

[23] B. Schiff, "Eigenvalues for ridged and other waveguides containing corners of angle $3\pi/2$ or 2π by the finite element method", *IEEE Trans. MTT* **39**, p. 1034, 1991.